Optimization of Control Parameter for Filter Algorithms for Attitude and Heading Reference Systems

Simone A. Ludwig
North Dakota State University
Fargo, ND, USA
simone.ludwig@ndsu.edu

***Abstract*—An Attitude and Heading Reference System (AHRS) provides orientation information of an object such as an Unmanned Air Vehicle by fusing sensor data from a magnetic and inertial measurement unit (MIMU). A MIMU consists of three components, which are a gyroscope, an accelerometer and a magnetometer. There are different fusion or filter algorithms available of which we have chosen the Mahony, the Madgwick, and the weighted filter. One of the shortcomings of all algorithms is that there is a control parameter involved in each which needs to be determined before applying the algorithms. Only an algorithm with an optimized control parameter achieves the best orientation information. Thus, a Particle Swarm Optimization algorithm is used to identify the control parameter of each filter algorithm. Experimental results show the influence the control parameter has on each algorithm.**

I. Introduction

Research focusing on the localization of objects and people has received significant attention in the past few decades. Numerous techniques have been proposed to achieve high-accuracy localization. GPS (Global Positioning System) is the most common technology, which provides accurate location in particular for outdoor environments, however, it suffers from signal blocking and the multipath effect. These effects lead to significant reduction in location accuracy and thus reduces the quality of the localization process. This is the main reason why other alternative sensor measuring techniques have been studied in order to overcome these location accuracy problems.

A magnetic and inertial measurement unit (MIMU) consists of a 3-axis MEMS gyroscope, accelerometer and magnetometer. MIMUs are widely used in many applications of attitude determination such as human motion tracking, unmanned aerial vehicle (UAV), mobile navigation, etc. [1]. The gyroscope measures the angular rate of a moving object, the accelerometer measures the acceleration of a certain object, and the magnetometer measures the magnetic field. However, low-cost sensors have inherent drawbacks [2], [3], such as nonlinearity, random walk, temperature drift, etc. In order to obtain a reliable attitude solution, MIMU sensor measurements have to be fused together using optimal sensor fusion algorithms [4].

The problem of attitude estimation is a well-known problem and has been extensively studied, particularly for devices whose motion is well-characterized. A survey of attitude estimation techniques for spacecrafts is given in [5]. Other attitude estimation techniques for pedestrian dead reckoning based on smartphone sensors is relatively new. However, the aim of all these attitude estimation systems is that the measurements obtained from a gyroscope, accelerometer, and magnetometer have to be combined. The different methods either use classical filtering methods such as Kalman filters (KFs) [6], extended Kalman filters (EKFs) [7], complementary filters [8], [9], [10], or observers [11].

In this paper, we have chosen to investigate the Mahony, the Madgwick, and the weighted filter due to their popularity. However, one of the shortcomings of all algorithms is that each has a control parameter that needs to be determined before applying the algorithms. Only an optimized control parameter achieves the best orientation information. Thus, an optimization technique referred to as Particle Swarm Optimization (PSO) is used to determine the best control parameters of the Mahony, Madgwick, and the weighted filter. Simulation experiments are run in order to investigate the influence the control parameter has on each algorithm.

II. Background to Magnetic and Inertial Measurement Unit (MIMU)

This section introduces the background of attitude estimation by first describing the attitude representation followed by the description of the sensors and their different types of noise.

A. Attitude Representation

With regards to the attitude representation, there are two different frames involved. One frame corresponds to the x, y, and z-axis of the object/device the MIMU is mounted on, referred to as $OF(OF_x, OF_y, OF_z)$, and the second frame represents the Earth frame, referred to as $EF(EF_x, EF_y, EF_z)$. In order for the tracking of objects to work, these two frames need to be aligned.

The attitude can be expressed by three different representations [12]. These are Euler angles (roll, pitch, yaw - see Figure 1), rotation matrix, or quaternion. A unit-norm quaternion, which essentially defines the rotation between EF and OF is defined as [13]:

$$q = S_{E_q} = \begin{bmatrix} q_0 \\ \overrightarrow{q} \end{bmatrix} = [q_0 \quad q_1 \quad q_2 \quad q_3]^T \in \Re^4 \tag{1}$$

where q_0 and $\overrightarrow{q}$ are the scalar and the vector portions of the quaternion, respectively.

The representation of Euler angles is comprised of three rotations [14]:

- a rotation φ around the x-axis (roll angle)
- a rotation θ around the y-axis (pitch angle)
- a rotation ψ around the z-axis (yaw angle)

The rotation matrix is a 3×3 matrix that represent the three unit vectors yielding 9 parameters used for attitude estimation.

Each of the three attitude representations has their advantages and disadvantages. For example, the Euler angle representation is subject to the gimbal-lock problem [14], and the rotation matrix contains 9 values that need to be determined, and quaternions are less intuitive to read and interpret. However, the quaternion representation avoids the singularity problem that is given by the Euler angles and in addition quaternions involve simple computations and thus can be operated on a large number of applications.

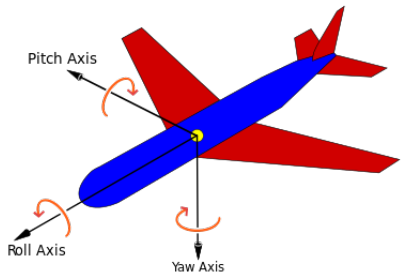

Fig. 1. Example of Roll, Pitch and Yaw [15]

B. MIMU Sensor

The Magnetic and Inertial Measurement Unit (MIMU) is composed of MEMS (Micro-Electro-Mechanical Systems) sensors that consists of a 3-axis accelerometer, a 3-axis gyroscope, and a 3-axis magnetometer. The sensor outputs of these low-cost sensors are not very good, meaning that they suffer from several problems such as noise, bias, scale factor, axis misalignment, axis non-orthogonality and local temperature [16].

1) Gyroscope: The gyroscope measures the angular velocity of the tracking object in $\frac{rad}{s}$ and is represented by: $[s_{w_x} \quad s_{w_y} \quad s_{w_z}]^T$. The gyroscope measurements suffer from:

- angular random walk
- bias instability
- rate random walk

The continuous time model for a gyroscope can be expressed such as:

$$s_w = s_{w_r} + s_{w_b} + s_{w_n} \tag{2}$$

where s_w is the angular rate measured by the gyroscope, s_{w_r} is the true angular rate, s_{w_b} is the gyroscope bias that models its derivative by a random walk noise, and s_{w_n} is the white noise of the gyroscope.

The gyroscope measurements are not enough for attitude estimation and thus additional sensors such as accelerometers and magnetometer can compensate this drift. The accelerometer corrects the pitch and roll angles, and the magnetometer improves the yaw angle.

2) Accelerometer: The accelerometer measures the sum of the gravity and external acceleration of the tracking object in $\frac{m}{s^2}$. The acceleration is given as $s_a = [s_{a_x} \quad s_{a_y} \quad s_{a_z}]^T$. As for the accelerometer measurements, the three main types of noise are:

- velocity random walk
- bias instability
- correlated noise

The continuous time model of the accelerometer can be summarized as:

$$s_a = s_{a_r} + s_{a_b} + s_{a_n} \tag{3}$$

where s_a is the sum of the gravity and external acceleration of the tracking object, s_{a_r} is the sum of the gravity and external acceleration, s_{a_b} is the accelerometer bias that models its derivative by a Gauss-Markov noise, s_{a_n} is the accelerometer white noise.

3) Magnetometer: The magnetometer measures the magnetic field of the tracking object in μT, and is represented as $s_m = [s_{m_x} \quad s_{m_y} \quad s_{m_z}]^T$. The Earth's magnetic field is modeled by a dipole and follows the basic laws of magnetic fields. At any location, the Earth's magnetic field can be represented by a three-dimensional vector. Please refer to [17] for more information.

The three types of noise of the magnetometer are:

- angle random walk
- bias instability
- correlated noise

The continuous time model of the magnetometer is represented as:

$$s_m = s_{m_r} + s_{m_b} + s_{m_n} \tag{4}$$

where s_m is the magnetic field measured by the magnetometer, s_{m_r} is the true magnetic field, s_{m_b} is the bias of the magnetometer where its derivate is modeled by a Gauss-Markov noise, and s_{m_n} is the white noise.

The magnetometer does not only measure the Earth's magnetic field, it is also influenced by magnetic disturbances caused by ferromagnetic objects in the environment.

III. Attitude Estimation Algorithms

The overall design of attitude estimation filters are described below. The Mahony filter [18], the Madgwick Filter [19], and the weighted filter [20] descriptions are provided.

A. Filter Design

The two algorithms are described using common notations used for quaternion and sensor readings. The estimated vector v is described by $\hat{v} = [\hat{v}_x \quad \hat{v}_y \quad \hat{v}_z]^T$, the quaternion and angular rate errors are given by q_e, w_e, and the time difference between 2 epochs is $\triangle t$.

The two filter algorithms use two reference vectors E_a and E_m in order to estimate q. In a noise-free environment, the relation between these two reference vectors are given as:

$$s_{a_q} = q^{-1} \otimes E_{a_q} \otimes q \tag{5}$$

where $\otimes$ is the quaternion multiplication [13]. s_{a_q} is the quaternion form of s_a, which can be written as $S_{a_q} = [0 \quad s_{a_x} \quad s_{a_y} \quad s_{a_z}]^T$. E_{a_q} is the quaternion form of E_a. For the static case it is $E_a = [0 \quad 0 \quad g]^T$ where g is the acceleration due to gravity ($g \approx 9.8\frac{m}{s^2}$).

In a perfect environment, one that is noise-free as well as there is no magnetic deviation, the relation between E_m and s_m is the following:

$$s_{m_q} = q^{-1} \otimes E_{m_q} \otimes q \tag{6}$$

where s_{m_q} is the quaternion form of s_m, which can be written as $s_{m_q} = [0 \quad s_{m_x} \quad s_{m_y} \quad S_{m_z}]^T$. E_{m_q} is the quaternion form of E_m. If there are no magnetic deviations, E_m can be calculated using [21].

The kinematic equation of a rigid body is defined by angular velocity measurements from a gyroscope to describe the variations of the attitude in terms of quaternions as such:

$$\dot{q} = \frac{1}{2} q \otimes s_{w_q} \tag{7}$$

where s_{w_q} is the quaternion of s_w.

B. Mahony Filter

Algorithm 1 displays the equations involved for the Mahony filter. Please note that k_i and k_p are the integral and proportional adjustable gains (see Equation 2). The algorithm computes the error by cross multiplying the measured and the estimated vectors, the acceleration and magnetic field, and then this error allows to correct the gyroscope bias.

Algorithm 1 Mahony Filter [18]

$s_{\hat{a}_{q,t}} = \hat{q}_{t-1}^{-1} \otimes E_{a_{q,t}} \otimes \hat{q}_{t-1}$
$s_{\hat{m}_{q,t}} = \hat{q}_{t-1}^{-1} \otimes E_{m_{q,t}} \otimes \hat{q}_{t-1}$

$s_{w_{mes,t}} = [s_{a_t} \times s_{\hat{a}_t}] + [s_{m_t} \times s_{\hat{m}_t}]$
$s_{\hat{w}_{b,t}} = -k_i s_{w_{mes,t}}$
$s_{\hat{w}_{r,q,t}} = s_{w_{q,t}} - [0 \quad s_{\hat{w}_{b,t}}] + [0 \quad k_p s_{w_{mes,t}}]$

$\dot{\hat{q}} = \frac{1}{2} \hat{q}_{t-1} \otimes s_{\hat{w}_{r,q,t}}$

Figure 2 shows the block diagram of the Mahony filter. An orientation error is obtained on the basis of the accelerometer and magnetometer measurements after the body orientation is computed at the previous step of the algorithm. Then, the measured angular velocity is corrected using a Proportional-Integral (PI) compensator. Afterwards, the quaternion propagation is integrated in order to obtain an estimate of the orientation after the quaternion normalization is completed.

C. Madgwick Filter

The algorithm of the Madgwick filter is shown in Algorithm 2. Madgwick is a gradient descent based algorithm where the quaternion error from the gradient descent algorithm provides also a gyroscope drift compensation. In the algorithm, J_t is the Jacobian Matrix of F_t, β is the divergence rate of q_t representing the magnitude of a quaternion derivative corresponding to the gyroscope measurement error, and ζ is the integral gain.

Algorithm 2 Madgwick Filter [19]

$E_{\hat{h}_{q,t}} = \hat{q}_{t-1} \otimes s_{m_{q,t}} \otimes \hat{q}_{t-1}^{-1}$
$E_{\hat{m}_{q,t}} = [0 \quad 0 \quad \sqrt{E_{\hat{h}_{x,t}}^2 + E_{\hat{h}_{y,t}}^2} \quad E_{\hat{h}_{z,t}}]^T$

$F_t = \begin{bmatrix} \hat{q}_{t-1}^{-1} \otimes E_{a_{q,t}} \otimes \hat{q}_{t-1} - s_{a_{q,t}} \\ \hat{q}_{t-1}^{-1} \otimes E_{m_{q,t}} \otimes \hat{q}_{t-1} - s_{m_{q,t}} \end{bmatrix}$

$\hat{q}_{e,t} = J_t^T F_t$

$s_{\hat{w}_{e,t}} = 2\hat{q}_{t-1} \otimes \hat{q}_{e,t}$
$s_{\hat{w}_{b,t}} = s_{w_{e,t}}$
$s_{\hat{w}_t} = s_{w_t} - \zeta s_{w_{b,t}}$

$\dot{\hat{q}}_t = \frac{1}{2} \hat{q}_{t-1} \otimes s_{\hat{w}_{q,t}} - \beta \frac{\hat{q}_{e,t}}{||\hat{q}_{e,t}||}$

Figure 3 shows the block diagram of the Madgwick filter. Two main process are used to compute the orientation of the rigid body. First, a correction algorithm is used to align the gyroscope measurements depending on the parameter. To minimize the effects that are due to the bias and the drift error, both are used to compute the body orientation via the quaternion propagation beginning from the orientation estimated at the previous step. Then, both the accelerometer and magnetometer measurements are fused together using a adjustable parameter, β, via the gradient descent algorithm as described in [14]. The output of the gradient descent algorithm is then used to correct the orientation estimated by considering the gyroscope measurements only.

D. Weighted Filter

The weighted filter approach consists of two components that are fused together as a weighted approach. The first part estimates the relative orientation obtained by integrating the gyroscope angular rate reading from an initial orientation [20]:

$$s_{w_{q,t}}^{-} = s_{w_{q,t-1}}^{+} \otimes \delta s_{w_{q,t}} \tag{8}$$

where $s_{w_{q,t}}^{-}$ is the quaternion orientation given by direct gyroscopic integration at sample time t, and $s_{w_{q,t-1}}^{+}$ represents a previous initial or fused estimation. The term $\delta s_{w_{q,t}}$ is the micro rotation given at the t^{th} sample interval measured by

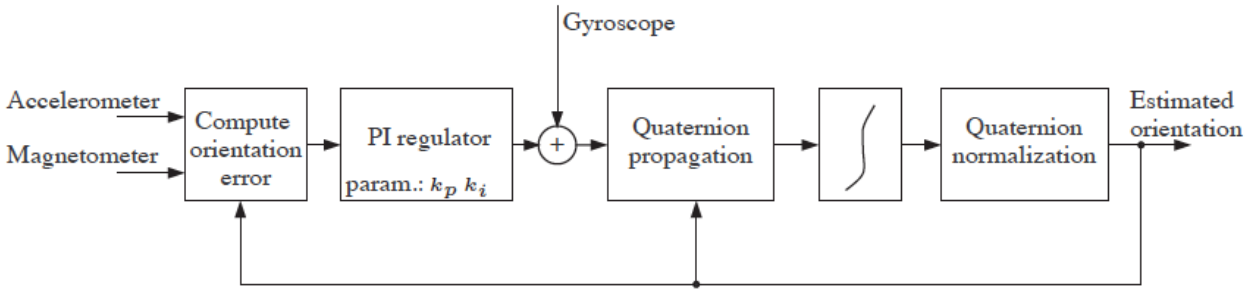

Fig. 2. Block diagram of Mahony Filter [16]

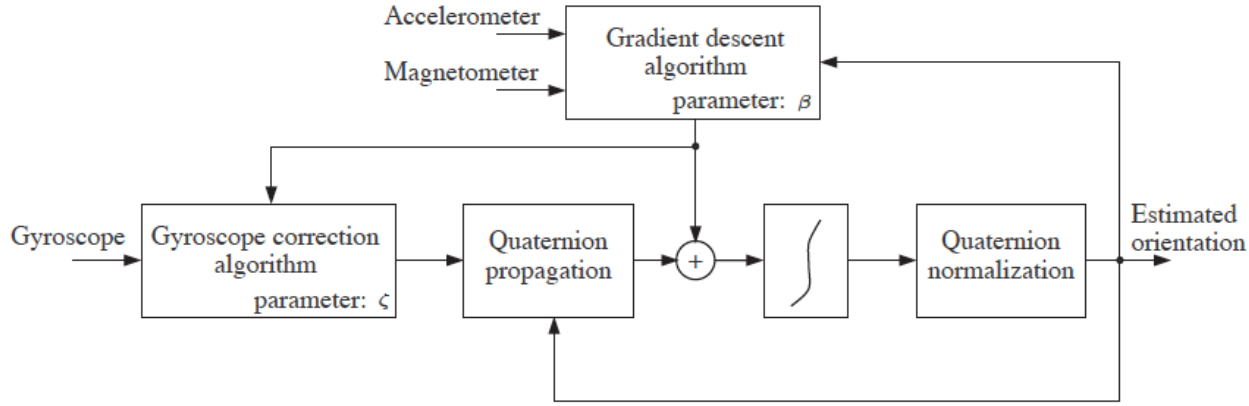

Fig. 3. Block diagram of Madgwick Filter [16]

the 3-axis gyroscope's angular rate s_w in radians per second. The term $\delta s_{w_{q,t}}$ is given by:

$$\delta s_{w_{q,t}} = [\cos(\tfrac{|s_w|dt}{2}), \sin(\tfrac{|s_w|dt}{2})\tfrac{s_{w_{q,1}}}{|s_w|}, \sin(\tfrac{|s_w|dt}{2})\tfrac{s_{w_{q,2}}}{|s_w|}, \sin(\tfrac{|s_w|dt}{2})\tfrac{s_{w_{q,3}}}{|s_w|}] \quad (9)$$

where $|s_w|$ is the norm of the gyroscope readings, and $s_{w_{q,1}}$, $s_{w_{q,2}}$ and $s_{w_{q,3}}$ are the three angular rates measured at time t.

The second component contributes the absolute orientation from the accelerometer and the magnetometer ($s_{q_{a/m,t}}$). As the gravity vector is known in magnitude and orientation, it is used to derive the absolute pitch and roll of the MIMU. The other euler angle (yaw) is derived by the known Earth magnetic vector, when projecting the magnetometer readings on a leveled plane using an electronic compass algorithm. These absolute pitch, roll and yaw angles ($s_{q_{a/m,t}}$) are noisy and subject to many interferences (sudden movements and magnetic perturbations).

Both components ($s^-_{w_{q,t}}$ and $s_{q_{a/m,t}}$) provide complementary orientation estimates and thus are fused together ($s^+_{w_{q,t}}$) in order to benefit from each source of information as given in Equation 10.

$$s^+_{w_{q,t}} = \gamma s^-_{w_{q,t}} + (1-\gamma) s_{q_{a/m,t}} \quad (10)$$

The expression contains the fusion of the gyro-based estimation with the absolute accelerometer/magnetometer drift-free correction by means of a time integration constant that is included in the γ term. Thus, the γ value provides the weighting between the gyroscope and the accelerometer/magnetometer in the equation.

IV. Experiments

In this section, the optimization tasks are described followed by an introduction of the optimization approach (particle swarm optimization), afterwards the sensor data description used for the experiments is provided, and then the results of the simulation experiments are outlined and discussed.

A. Optimization Approach: Particle Swarm Optimization

The optimization method referred to as Particle Swarm Optimization (PSO) is part of a group called swarm intelligence methods. PSO is a population-based stochastic search technique [22]. The main idea behind PSO is the continuous search of the population (swarm) for better solutions whereby each particle participates in the process. The algorithm starts with the initialization of a population of random solutions. Each particle is assigned a random velocity that determines the direction that the particle will search for, and each particle keeps track of the coordinates that are associated with its solution, which is calculated based on the fitness function.

During every iteration all particles move based on the following equations:

$$\mathbf{x}^{(i)}(n+1) = \mathbf{x}^{(i)}(n) + \mathbf{v}^{(i)}(n+1), \quad n = 0, 1, 2, \ldots, N-1 \tag{11}$$

where $\mathbf{x}^{(i)}$ is the position of particle i, n is the iteration number with $n = 0$ referring to the initialization, N is the total number of iterations, and $\mathbf{v}^{(i)}$ is the velocity of particle i, $i = 1, 2, \ldots, n_p$, where n_p is the number of particles. Classical PSO uses the following iteration to update the particle velocities:

$$\begin{aligned}\mathbf{v}^{(i)}(n+1) = \mathbf{v}^{(i)}(n) &+ 2\mathbf{r}_1^{(i)}(n)[\mathbf{x}_p^{(i)}(n) - \mathbf{x}^{(i)}(n)] \\ &+ 2\mathbf{r}_2^{(i)}(n)[\mathbf{x}_g(n) - \mathbf{x}^{(i)}(n)], \\ n &= 0, 1, 2, \ldots, N-1\end{aligned} \tag{12}$$

where $\mathbf{x}_p$ is the personal best position, and $\mathbf{x}_g$ is the global best position. Both $\mathbf{r}_1^{(i)}$ and $\mathbf{r}_2^{(i)}$ are vectors with components having random values uniformly distributed between 0 and 1. The notation $\mathbf{r}^{(i)}(n)$ denotes a new random vector generated for every particle i and every iteration n.

B. PSO-Optimized Parameter Optimization

The PSO algorithm is applied to the Mahony, Madgwick, and weighted filter. One control parameter (optimization constant) each is to be optimized for each filter. The optimization constant for the Mahony filter is the k_i and k_p ratio, whereas the optimization constant for the Madgwick filter is β. As for the weighted filter, γ needs to be optimized to achieve the best orientation results. Thus, the steps of the optimization are explained using the term 'optimization constant' referring to each filter algorithm. First, the problem (optimization constant) needs to be encoded using a particle representation, and a fitness equation needs to be defined (in our case it is the filter calculation for Mahony, Madgwick, weighted filter, respectively). The inertial weight w as well as the acceleration constants C_1 and C_2 need to be assigned ($w = 1.4$, $C_1 = C_2 = 2$). The overall flow of the algorithm is as follows: first, a randomly generated swarm is initialized, then the fitness of each particle (solution) is evaluated, afterwards the two PSO equations (Equations 11 and 12) are executed and the personal best and global best values are being kept track of and the next iteration begins. The algorithm terminates once the maximum number of iterations has been reached.

C. Data Description

The data used is foot mounted MIMU measurement data [23] that is freely available. It contains sensor data of a straight trajectory of $1,000$ steps based on a human step pattern characteristics measured by a motion capture system. For our experiments, we have only used partial data of the data set. The information from the MIMU is the acceleration, turn rates from the gyroscope and the magnetic field. The data set includes the orientation (Euler and DCM) ground truth values. The units are in meters, seconds and radians, a sampling frequency of 100 Hz was used, and gravity is $9.8\frac{m}{s^2}$.

As the dataset with orientation ground truth is noiseless, we have added a typical real noise content to the dataset. This noise was generated from a very common MEMS MIMU, XSense MTi unit, by keeping it still during several hours. So different noise windows can be used in order to get different bias conditions and instabilities. The noise patterns have the following features:

- Accelerometer: $0.012\frac{m}{s^2}$ standard deviation random noise and a random constant with a Gaussian distribution and a standard deviation of $0.04\frac{m}{s^2}$ for the bias.
- Gyroscope: $0.0087\frac{rad}{s}$ standard deviation random noise and a random constant with a Gaussian distribution and a standard deviation of $0.015\frac{rad}{s}$ for the bias.

XSense MIMU are commonly used in motion sensing applications, and are seen as the gold standard for scientific research [24]-[26].

Figure 4 shows the sensor data obtained by the gyroscope, accelerometer, and magnetometer. The cyclic steps of the walking motion can be observed.

D. Simulation Experiments

Different configurations of the PSO algorithm were run, but the one that resulted in the best run is the following:

- Size of a swarm = 30
- w = 1.4
- C_1 = 2
- C_2 = 2
- Number of iterations = 30

E. Results

An example of the performance plot of the optimization process for the weighted filter, whereby γ is optimized, is shown in Figure 5. Both, the best RMSE (Root Mean Square Error) as well as the average RMSE of the PSO swarm is shown. As can be seen, the RMSE value of the best particle converges to a value of 2.621.

Table I lists the best optimization values for each filter algorithm. The following figures and table show the results based on the best optimization values obtained (given in Table I).

TABLE I
BEST OPTIMIZATION VALUE OF ALL THREE FILTERS

	Mahony (k_i / k_p)	Madgwick (β)	Weighted (γ)
best	0.0221	0.0588	0.9885
worst	0.1922	0.1059	1.0

Figure 6 shows the Euler estimation correctness of Mahony, Madgwick and the weighted filter, respectively. The figures show the estimated values and the ground truth values for roll, pitch, and yaw, respectively. However, since it is difficult to judge which filter algorithm is the best, the RMSE values are usually more meaningful.

Table II lists the RMSE values of roll, pitch, yaw and norm results for all filters. The results reveal that the RMSE values

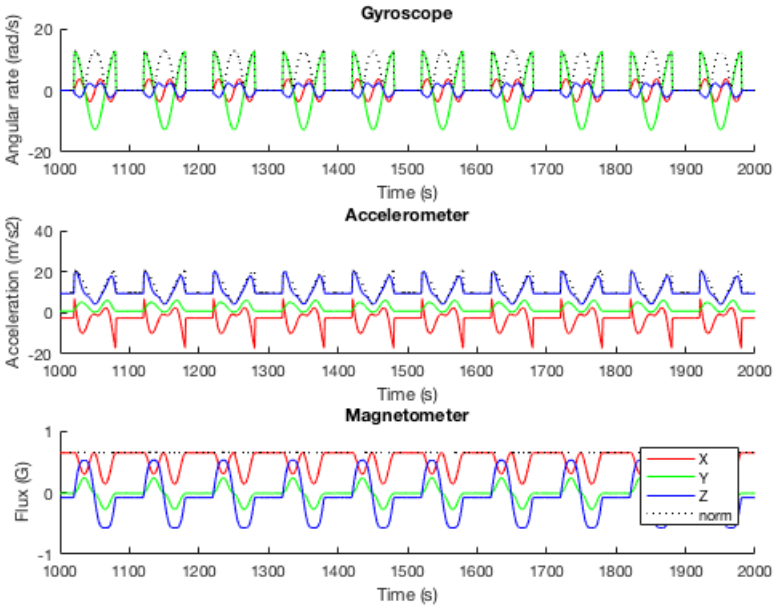

Fig. 4. Sensor data of gyroscope, accelerometer, magnetometer

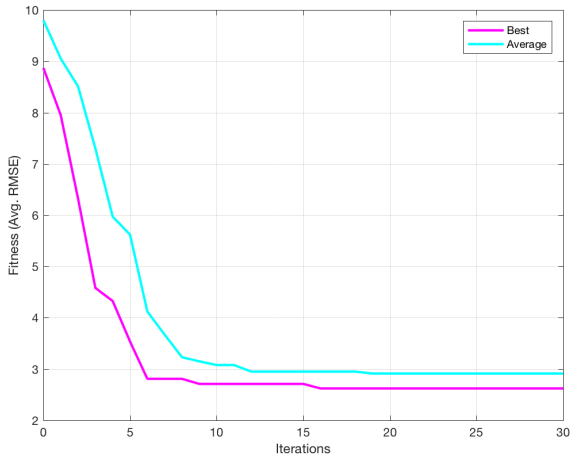

Fig. 5. Comparison of Performance plot of Weighted Filter

of the Mahony and Madgwick filter are comparably good with Madgwick slightly outperforming the Mahony filter. The weighted filter has the highest norm RMSE value of 4.7759.

TABLE II
RMSE VALUES OF ROLL, PITCH, YAW AND NORM RESULTS FOR ALL FILTERS

	roll	pitch	yaw	norm
Mahony	0.1333	0.6329	0.0109	0.6469
Madgwick	0.1440	0.6241	0.0053	0.6405
Weighted	2.1354	3.5662	2.3520	4.7759

Table III lists the norm RMSE improvement when the best optimization value, k_i / k_p, β, and γ is used compared to the worst for Mahony, Madgwick, and the weighted filter, respectively. As can be seen from the values, the best results are achieved for the weighted filter with an improvement of 28.5% whereas the Mahony and Madgwick filter only benefit slightly from the optimization of their respective optimization constants.

TABLE III
NORM RMSE IMPROVEMENT WHEN BEST OPTIMIZATION VALUE IS USED

	worst	best	improvement [%]
Mahony	0.6598	0.6469	1.0199
Madgwick	0.657	0.6405	1.0257
Weighted	136.116	4.7759	28.5006

V. CONCLUSION

Past research work has developed different fusion or filter algorithms of which we chose the Mahony, the Madgwick, and the weighted filter to be used for our investigation. One of the shortcomings of all these filter algorithms is that there is a control parameter involved in each of them, which needs to be determined before the algorithm is applied. Only a filter algorithm with an optimized control parameter achieves the best orientation information. Thus, a Particle Swarm Optimization (PSO) algorithm was used to identify the best control parameter of each filter algorithm.

The simulation experiments were run with the PSO algorithm optimizing the control parameter of each filter algorithm, and once the best parameter was obtained, the corresponding

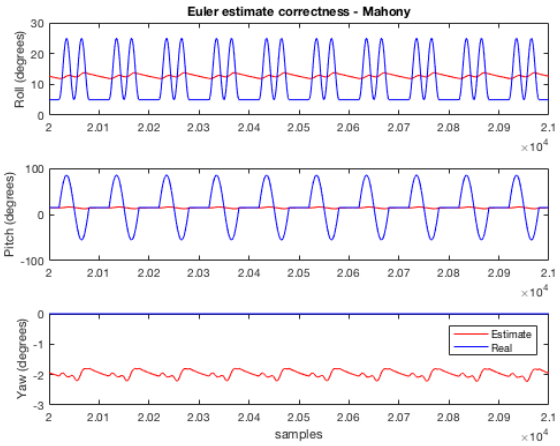

(a) Mahony

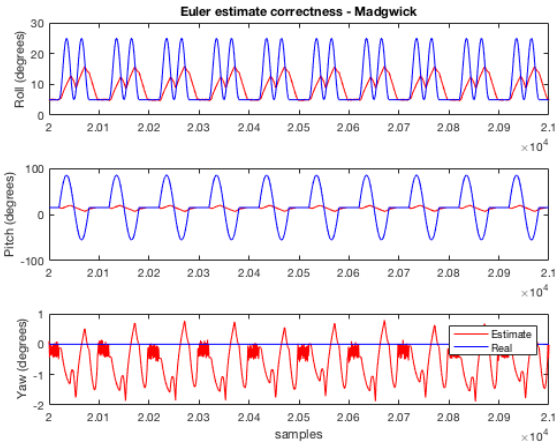

(b) Madgwick

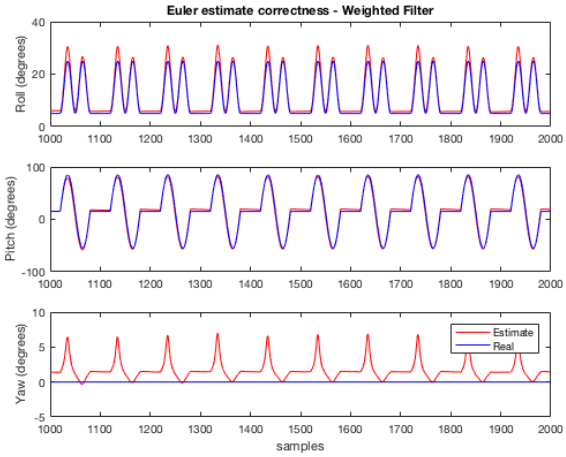

(c) Weighted Filter

Fig. 6. Comparison of Euler estimation correctness of Mahony, Madgwick, and Weighted Filter

filter was run in order to acquire the orientation information in the form of RMSE values for roll, pitch, yaw, and the norm as well as the Euler estimation correctness. The results revealed that the PSO optimization was most effective on the weighted filter approach. Comparing the RMSE norm values using the worst or best γ value resulted in an improvement of 28.5%. The norm RMSE improvements for the Mahony and Madgwick filter however were more moderate, thus, not having a big impact on the orientation information. Overall, the Mahony and Madgwick filter proved to be the best choices in terms of orientation information with norm RMSE values of 0.6469 and 0.6405, respectively.

Future work will investigate the Extended Kalman Filter applied to the data set. In addition, related work has also applied the Unscented Kalman filter, which shows promise in particular for this area of research.

ACKNOWLEDGMENT

This work is funded by North Dakota Department of Commerce under project number FAR0027254.

REFERENCES

[1] H. Fourati, Heterogeneous data fusion algorithm for pedestrian navigation via foot-mounted inertial measurement unit and complementary filter, IEEE Trans. Instrum. Meas., vol. 64, no. 1, pp. 221-229, Jan. 2015.

[2] N. Barbour, G. Schmidt, Inertial sensor technology trends, IEEE Sensors J., vol. 1, no. 4, pp. 332-339, Dec. 2001.

[3] J. Leclerc, MEMS for aerospace navigation, IEEE Aerosp. Electron. Syst. Mag., vol. 22, no. 10, pp. 31-36, 2007.

[4] A. Makni, H. Fourati, A. Y. Kibangou, Energy-aware adaptive attitude estimation under external acceleration for pedestrian navigation, IEEE/ASME Trans. Mechatronics, vol. 21, no. 3, pp. 1366-1375, Jun. 2016.

[5] J. L. Crassidis, F. L. Markley, and Y. Cheng, Survey of nonlinear attitude estimation methods, Journal of Guidance, Control, and Dynamics, vol. 30, no. 1, pp. 12-28, 2007.

[6] D. Choukroun, I. Y. Bar-Itzhack, and Y. Oshman, Novel quaternion kalman filter, Aerospace and Electronic Systems, IEEE Transactions on, vol. 42, no. 1, pp. 174-190, 2006.

[7] V. Renaudin and C. Combettes, Magnetic, acceleration fields and gyroscope quaternion (MAGYQ)-based attitude estimation with smartphone sensors for indoor pedestrian navigation, Sensors, vol. 14, no. 12, pp. 864-890, 2014.

[8] R. Mahony, T. Hamel, and J.-M. Pflimlin, Nonlinear complementary filters on the special orthogonal group, Automatic Control, IEEE Transactions on, vol. 53, no. 5, pp. 1203-1218, 2008.

[9] S. O. Madgwick, A. J. Harrison, and R. Vaidyanathan, Estimation of IMU and MARG orientation using a gradient descent algorithm, in 2011 IEEE International Conference on Rehabilitation Robotics (ICORR), 2011, pp. 1-7.

[10] H. Fourati, Heterogeneous data fusion algorithm for pedestrian navigation via foot-mounted inertial measurement unit and complementary filter, Instrumentation and Measurement, IEEE Transactions on, vol. 64, no. 1, pp. 221-229, Jan 2015.

[11] P. Martin and E. Salaun, Design and implementation of a lowcost observer-based attitude and heading reference system, Control Engineering Practice, vol. 18, no. 7, pp. 712-722, 2010.

[12] D. Sachs, Sensor fusion on android devices: A revolution in motion processing, [Video] https://www.youtube.com/watch?v=C7JQ7Rpwn2k, 2010, [Online; last accessed December 2017].

[13] B. Kuipers, Quaternions and rotation sequences, 1999, vol. 66.

[14] J. Diebel, Representing attitude: Euler angles, unit quaternions, and rotation vectors, Matrix, vol. 58, pp. 15-16, 2006.

[15] https://en.wikipedia.org/wiki/Euler_angles

[16] T. Michel, H. Fourati, P. Geneves, N. Layada. A Comparative Analysis of Attitude Estimation for Pedestrian Navigation with Smartphones. 2015 International Conference on Indoor Positioning and Indoor Navigation, Banff, Canada, October 2015.

[17] W. M. Chung, S. Yeung, W. W. Chan, R. Lee, Validity of VICON Motion Analysis System for Upper Limb Kinematic Measurement A Comparison Study with Inertial Tracking Xsens System. Hong Kong Physiother. J. 2011.

[18] R. Mahony, T. Hamel, and J.-M. Pflimlin, Nonlinear complementary filters on the special orthogonal group, Automatic Control, IEEE Transactions on, vol. 53, no. 5, pp. 12031218, 2008.

[19] S. O. Madgwick, A. J. Harrison, and R. Vaidyanathan, Estimation of IMU and MARG orientation using a gradient descent algorithm, in 2011 IEEE International Conference on Rehabilitation Robotics (ICORR), 2011.

[20] E. Muñoz, A. R. Jiménez, F. de Ponte, F. Zampella, Evaluation of AHRS Algorithms for Inertial Personal Localization in Industrial Environments, Proceedings of the 2015 IEEE International Conference on Industrial Technology (ICIT), pp. 3412 - 3417 Seville, Spain, March 17-19, 2015.

[21] NGA and the U.K.'s Defence Geographic Centre (DGC), The world magnetic model, http://www.ngdc.noaa.gov/geomag/WMM, 2015, [Online; last accessed December 2017].

[22] J. Kennedy, R. C. Eberhart, Particle swarm optimization, Proceedings of IEEE International Conference on Neural Network, Perth, pp. 1942-5, 1995.

[23] Foot Mounted IMU data sets for the evaluation of PDR algorithms, LOPSI Research group, Spain, http://lopsi.weebly.com/downloads.html, 2017.

[24] A. G. Cutti, A. Giovanardi, L. Rocchi, A. Davalli, R. Sacchetti, Ambulatory measurement of shoulder and elbow kinematics through inertial and magnetic sensors. Med. Boil. Eng. Comput., 46, 169-178, 2008.

[25] D. Hamacher, D. Bertram, C. Folsch, L. Schega, Evaluation of a visual feedback system in gait retraining: A pilot study. Gait Posture, 36, 182-186, 2012.

[26] K. Saber-Sheikh, E. C. Bryant, C. Glazzard, A. Hamel, R. Y. Lee, Feasibility of using inertial sensors to assess human movement. Man. Ther., 15, 122-125, 2010.